Available online at www.sciencedirect.com
ScienceDirect
Geochimica et Cosmochimica Acta 70 (2006) 4095–4104
Geochimica
www.elsevier.com/locate/gca

Insights for size-dependent reactivity of hematite nanomineral surfaces through Cu^{2+} sorption

Andrew S. Madden [a,*], Michael F. Hochella Jr. [a], Todd P. Luxton [b]

[a] *NanoGeoscience and Technology Laboratory, Department of Geosciences, Virginia Tech, Blacksburg, VA 24061, USA*
[b] *Department of Crop, Soil, and Environmental Science, Virginia Tech, Blacksburg, VA 24061, USA*

Received 11 July 2005; accepted in revised form 16 June 2006

Abstract

Macroscopic sorption edges for Cu^{2+} were measured on hematite nanoparticles with average diameters of 7 nm, 25 nm, and 88 nm in 0.1 M $NaNO_3$. The pH edges for the 7 nm hematite were shifted approximately 0.6 pH units lower than that for the 25 nm and 88 nm samples, demonstrating an affinity sequence of 7 nm > 25 nm = 88 nm. Although, zeta potential data suggest increased proton accumulation at the 7 nm hematite surfaces, changes in surface structure are most likely responsible for the preference of Cu^{2+} for the smallest particles. As Cu^{2+} preferentially binds to sites which accommodate the Jahn–Teller distortion of its coordination to oxygen, this indicates the relative importance of distorted binding environments on the 7 nm hematite relative to the 25 nm and 88 nm particles. This work highlights the uniqueness of surface reactivity for crystalline iron oxide particles with decreasing nanoparticle diameter.

1. Introduction

Nanoscale (hydr)oxide minerals, those having physical dimensions of approximately 1–50 nm, are common constituents of the natural world (Bigham et al., 2002). Over this length scale, materials have properties that are dependent on the particle size (Hochella, 2002; Gilbert and Banfield, 2005). In particular, the relationships between iron oxide mineral sizes and their properties as related to geochemical reactivity are just beginning to be explored. Iron oxides are involved in a wide variety of geochemical processes, including sorption of metals, acceptance of electrons from microbial respiration, photochemical reduction, and heterogeneous catalysis. Nanoscale iron oxide particles with surface-bound metals are found many kilometers downstream from mining sites, suggesting their importance to colloid-mediated transport of sorbed contaminants (Hochella et al., 2005a,b). Any and all of these processes are likely to show size-dependent reactivity on crystalline iron oxide nanoparticles, such that each process will occur with different thermochemical and kinetic relationships as a function of size. For example, Mn^{2+} oxidation rates on 7 nm average diameter hematite particles were shown to be up to two orders of magnitude faster than on those with average diameter 37 nm, even when normalized to surface area (Madden and Hochella, 2005). Based on arguments from electron transfer theory, it was hypothesized that the rate differences may be related to changes in the coordination environment for Mn^{2+} adsorbed on the different sizes of hematite, specifically a decrease in symmetry of the coordination complex. The decrease in symmetry was hypothesized to stabilize Mn^{3+} ($3d^4$ electron configuration) relative to Mn^{2+} ($3d^5$ electron configuration).

Other concurrent work on iron oxide nanoparticles has demonstrated a change in the distribution of binding environments as a function of size. Waychunas et al. (2005) studied the sorption of trace and heavy metals on goethite-like iron oxide nanoparticles with X-ray absorption fine structure (EXAFS). The simplest explanation to describe the changes in metal–Fe distances observed in the EXAFS spectra is that there is a decrease in the symmetry

* Corresponding author. Present address: Environmental Sciences Division, Oak Ridge National Laboratory, P.O. Box 2008, Oak Ridge, TN 37831-6036, USA.
E-mail address: maddsenas@ornl.gov (A.S. Madden).

0016-7037/$ - see front matter © 2006 Elsevier Inc. All rights reserved.
doi:10.1016/j.gca.2006.06.1366

of bonding environments on the smallest particles relative to the larger particles. In addition, molecular dynamics simulations performed by Rustad and Felmy (2005) found that certain edges of 2–8 nm goethite nanoparticles give rise to potential binding sites with longer Fe—O_{water} bond lengths and thus increased Lewis base character. These specific edge sites would be most susceptible to electron transfer reactions.

Mineral surface defects, topographic features, and step/particle edges are known to control many aspects of reactivity at the mineral–water interface, yet it remains challenging to directly probe their atomic and electronic structure in solution (Hochella, 1990; Brown and Parks, 2001). Some progress has been made with the evolution of aqueous phase tunneling microscopy (e.g., Eggleston et al., 2003) and theoretical modeling (e.g., Becker et al., 1996). Undercoordinated surface metal atoms and related oxygen vacancies are clearly key to many aspects of industrial catalysis of gas-phase molecules on transition metal oxides (Kim et al., 1979; Henrich and Cox, 1996; Sadykov et al., 2000). Undercoordinated surface atoms are known to exist in greater proportion on oxide nanoparticles in vacuum as the particle size decreases (Clementz et al., 1973; Chen et al., 1997, 2002; Rajh et al., 2002; Zhang et al., 2003; Fernandez-Garcia et al., 2004).

Studies on model materials such as MgO (Stirnman et al., 1996; Liu et al., 1998a; Chiesa et al., 2005) and more geochemically relevant materials such as iron sulfides and oxides (Becker et al., 1996; Henderson et al., 1998; Rosso et al., 2000; Becker and Rosso, 2001; Rosso, 2001; Borda et al., 2003; Elsetinow et al., 2003) have begun to provide fundamental information on the role that defects and undercoordinated surface metal atoms play in the chemical reactivity of surfaces. Certainly hematite surfaces are known to have heterogeneous surfaces, including topographic features and defects, such that only certain portions of the surface will be reactive to any given geochemical process (Junta-Rosso and Hochella, 1996; Junta-Rosso et al., 1997; Liu et al., 1998b; Samson and Eggleston, 1998; Wang et al., 1998; Samson and Eggleston, 2000; Eggleston et al., 2003, 2004; Trainor et al., 2004). When the dimensions of the particles are less than approximately 10 nm, an increasingly large proportion of the surface would be expected to deviate from a flat terrace. Metal binding at edges, steps, and other surface features will be influenced by the local atomic and electronic structure associated with the unique arrangement of surface atoms present.

In this study, Cu^{2+} ions are used to probe the nature of binding sites on hematite nanoparticles. Cu^{2+} serves as an excellent probe for distorted binding environments. With a $3d^9$ electron configuration, it experiences Jahn–Teller distortion in octahedral coordination, similar to Mn^{3+}, as evidenced in solution (Baes and Mesmer, 1986), complexed with humic acid (e.g., Xia et al., 1997; Alcacio et al., 2001), and on mineral surfaces (e.g., McBride, 1989; Parkman et al., 1999; Cheah et al., 2000; Scheinost et al. Peacock and Sherman, 2004). Although Cu^{2+} binds s ly to oxide surfaces, it also fractionates strongly to c ed binding sites that are common in natural organic (McBride, 1981; Buerge-Weirich et al., 2002). If the est hematite nanoparticles have more distorted b sites for Cu^{2+}/m^2 of mineral surface area, we would to measure a shift in the pH-dependent sorption bel of Cu^{2+} which is dependent on particle size.

In addition to its use as a surface probe species also important to keep in mind that the sorption on oxide surfaces is an important control of Cu dis tion in the environment along with complexatic organic matter (James and Barrow, 1981; Mcl 1981; Kabata-Pendias and Pendias, 1992). Althoug is an essential micronutrient, it is toxic at relatively concentrations. For heavy metals, the copper to threshold for algae, flowering plants, fungi, and p plankton is only surpassed by Hg and sometime (Sposito, 1989). Cu has been documented to be assoc with nanoscale iron oxide surfaces in relation to m activities (Hochella et al., 1999, 2005b).

2. Materials and methods

2.1. Particle synthesis and characterization

2.1.1. Hematite synthesis

Two synthetic hematite samples were prepared in laboratory, loosely following the instructions from met 1 and method 4 of Schwertmann and Cornell (2000). L er hematite particles were synthesized by bringing an Er meyer flask containing 500 mL of 0.002 M HCl to a boi a hot plate. After bringing the solution to a boil, 4.04 $Fe(NO_3)_3 \cdot 9H_2O$ was added and the flask was vigoro shaken. Immediately, the flask was returned to the l and held at a very mild boil for 7 days, periodically rep ing evaporated water.

The smaller hematite nanoparticles were synthesi (method 4, (Schwertmann and Cornell, 2000)) by slo dripping 60 mL of 1 M ferric nitrate solution from a b ette into 750 mL water boiling on a hot plate. After the c solution was consumed, the nanoparticle suspension v removed from heat.

Dialysis tubing was rinsed several times in MilliQ wa baths at least one day prior to adding sample. Cooled s pensions were dialyzed against MilliQ water until the co ductivity of the dialysis water nearly reached that of pu MilliQ. For the smallest particles (method 4), a final dia sis was performed against pH 4 MillQ water, adjusted w HNO_3.

An additional synthetic commercial sample was al used. Anhydrous ferric oxide (Fisher Scientific) was us without further treatment. Impurities were listed 0.002%, nitrate 0.01%, phosphate 0.005%, sulfate 0.07 Mn 0.02%, Cu 0.002%, Zn 0.008%, substances not preci itated by NH_4OH 0.08%.

2.1.2. Characterization

Transmission electron microscopy (TEM) was used to determine the shape and diameter of the particles. Mineral suspensions were dropped onto formvar/carbon coated Cu grids and allowed to dry. Dried grids were imaged in a Phillips EM 420T TEM. Negatives of images and diffraction patterns were scanned for subsequent image analysis.

The height dimension of the particles was measured with atomic force microscopy (AFM). Dilute mineral suspensions were dropped onto Si wafer chips and heated briefly at 60 °C in an oven. The remaining suspension was blotted with a kimwipe. Images were collected in contact mode with oxide-sharpened SiN tips. Images were flattened (with exclusion of particle areas) before height analysis.

The surface area for the smallest particles was determined geometrically using 2D measurements from TEM negatives and height measurements by AFM (Madden and Hochella, 2005). Briefly, a size distribution was generated in 1 nm histogram bins. The particles were assumed to be irregular hexagonal plates (both length and width measured in TEM negatives), and the surface area was calculated for a particle in each histogram bin. The total surface area is obtained by multiplying the surface area of an average particle from each bin by the fraction of the total particles represented by that bin. Surface area of the commercial sample was measured with a 6-point BET N_2 isotherm after degassing for 24 h at 80 °C.

Powder X-ray Diffraction (XRD) was performed using a Scintag powder X-ray diffractometer using Cu radiation and a step size of 0.02 degrees 2θ.

For determination of the particle surface potential, mineral suspensions (0.5 g/L) were prepared with 0.01 M NaCl in tubes individually adjusted to various pH values. Zeta potential measurements were conducted from microeletrophoresis measurements collected using a Malvern Zetasizer 3000 HSa. Based on preliminary data and particle size, the voltage applied to the capillary cell was set at 200 mV and a Henry function ($f(K_a)$) of 1.5 was used to calculate the zeta potential.

2.2. Batch sorption experiments

Batch sorption experiments were performed in a Teflon beaker contained within a custom-designed glass reaction vessel. N_2 gas was passed through an O_2 trap and hydrating CO_2 trap before bubbling into the reactor. A floating Teflon magnetic stir bar provided agitation. Positive pressure, necessary for CO_2 exclusion, was observed using a gas outlet port leading to a water-filled beaker. A Radiometer pHC3006 Ag/AgCl combination electrode provided pH measurement. Cu was added as solid $CuCl_2 \cdot 2H_2O$. Solutions used to adjust pH were 0.1 M HNO_3, 0.1 M NaOH, and 0.001 M NaOH. Reactions occurred at room temperature, measured to be 20.5–21.5 °C. Equilibration time for each sample in these experiments was 50 ± 5 min. Samples were extracted and centrifuged at forces up to 140,000 rcf for 15 min at 4 °C before preservation in HCl. Metal concentrations were measured by ICP-AES. $NaNO_3$ (0.1 M) was chosen as the electrolyte. Copper sorption has been shown to have ionic strength dependencies (Rose and Bianchi-Mosquera, 1993) for Cu sorption onto quartz (Criscenti and Sverjensky, 1999); however, no ionic strength dependence has been observed for Cu sorption on iron oxides in nitrate electrolytes (Swallow et al., 1980; Jung et al., 1998). Additional experimental details are listed in Table 1.

3. Results and discussion

3.1. Particle characteristics

Average diameters for the particles are 7 nm, 25 nm (synthetic samples from our laboratory), and 88 nm (Fisherbrand sample). Average heights of the 7 nm and 25 nm samples were measured to be 1.4 nm and 4.8 nm. The shapes of the two smaller samples are pseudo-hexagonal, as observed by TEM (Fig. 1a and b), while the commercial sample is more irregular (Fig. 1c). Diffraction patterns of 7 nm and 25 nm samples have only d-spacings characteristic of hematite (Fig. 2, top), while the Fisher sample pattern is characteristic of hematite with maghemite (γ-Fe_2O_3) present as a minor impurity (Fig. 2, bottom). The XRD patterns for the 7 nm and 25 nm samples exhibit peak broadening, an expected phenomenon (Waychunas, 2001). Surface areas were calculated for the in-house synthetic samples as 188 m^2/g and 62 m^2/g for the 7 nm and 25 nm hematite, respectively. Surface area for the 88 nm particles was measured to be 9.1 m^2/g.

Table 1
Details for batch copper sorption experiments

	7 nm (1)	7 nm (2)	25 nm	25 nm	88 nm
Volume (L)	0.4	0.4	0.5	0.4	0.5
g $NaNO_3$	3.52	3.52	4.4	3.99	4.788
mol/L $NaNO_3$	1.0E−01	1.0E−01	1.0E−01	1.2E−01	1.1E−01
mol/L Cu^{2+}	4.5E−05	4.1E−05	2.933E−05	7.772E−05	2.933E-05
Susp. density (g/L)	0.25	0.25	0.85	0.6	0.85
Surface area (m^2/g)	188	188	62	62	9.1
Total mol Cu^{2+}	1.8E−05	1.6E−05	1.5E−05	3.1E−05	1.5E−05
mol Cu^{2+}/m^2	9.7E−07	8.7E−07	5.6E−07	2.1E−06	3.8E−06

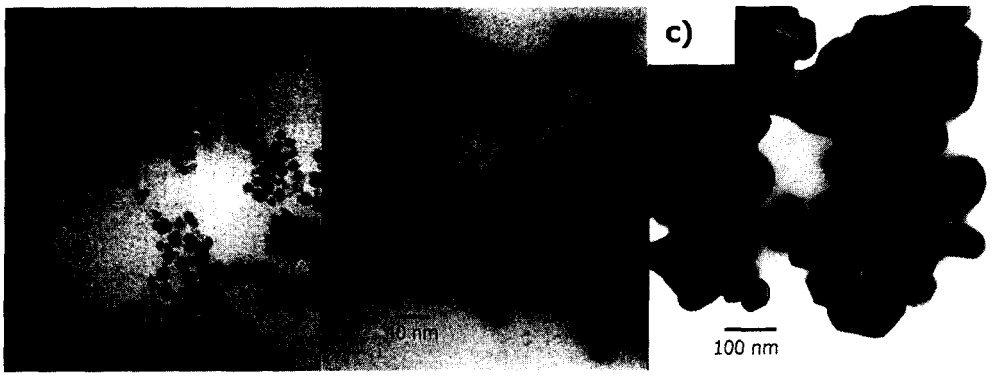

Fig. 1. TEM images of the (a) 7 nm average diameter, (b) 25 nm average diameter hematite, and (c) Fisherbrand 88 nm average diameter samples.

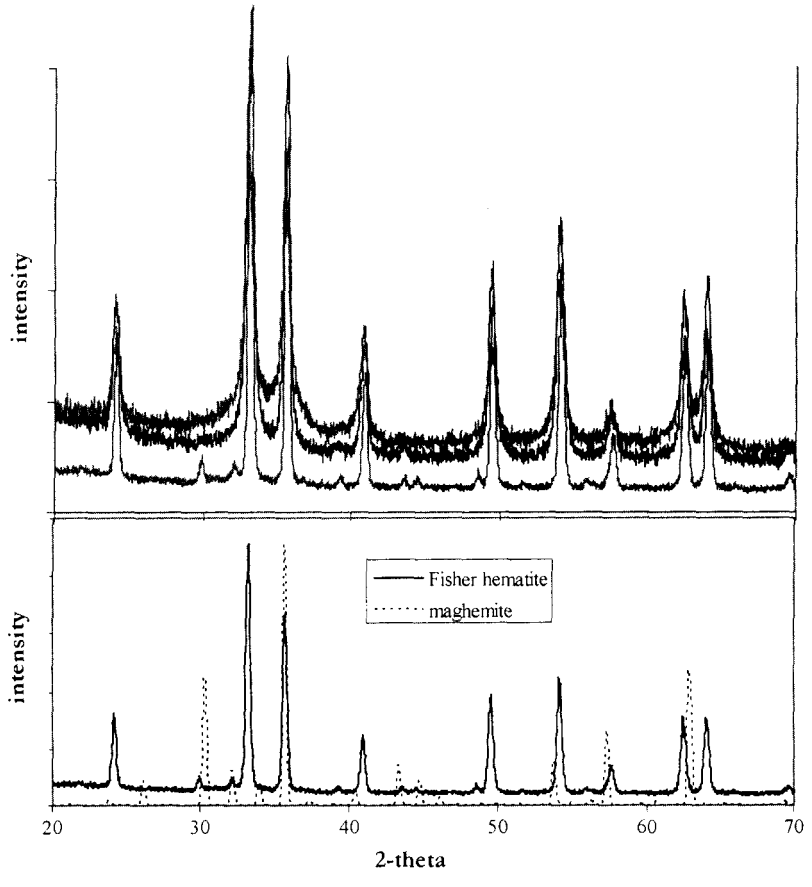

Fig. 2. Top: XRD patterns of 7 nm (higher background), 25 nm (middle), and Fisherbrand (88 nm, bottom) hematite. Bottom: comparison of XRD pattern from Fisherbrand sample with an idealized maghemite pattern using data from Pecharroman et al. (1995).

3.2. Cu sorption

Macroscopic sorption edges of Cu^{2+} on hematite nanoparticles are shown as percent Cu sorbed/m^2, normalized to the highest sorption value in each experiment (Fig. 3). The data in Fig. 3 represent initial Cu to surface ratios of 0.97, 0.87, and 0.56 μmol Cu/m^2 for the two 7 nm and the 25 nm hematite experiments. Additionally, pH edges are presented corresponding to higher Cu^{2+} Cu:surface ratios of 2.1 μmol Cu/m^2 on the 25 nm particles and 3.8 μmol Cu/m^2 on the 88 nm particles (data summarized in electronic annex EA-1). Data for the 7 nm average diameter particles represent the combination of two separate experimental runs, while the other data sets correspond to separate experiments.

All samples analyzed for Cu were also analyzed for Fe. The presence of Fe is evidence that some particles were retained in the supernatant after centrifugation or resuspended during supernatant removal. As the pH increases through the edge, these extra particles will have bound Cu that will influence the data in Fig. 3. However, the total amount of Cu that is calculated to be associated with the

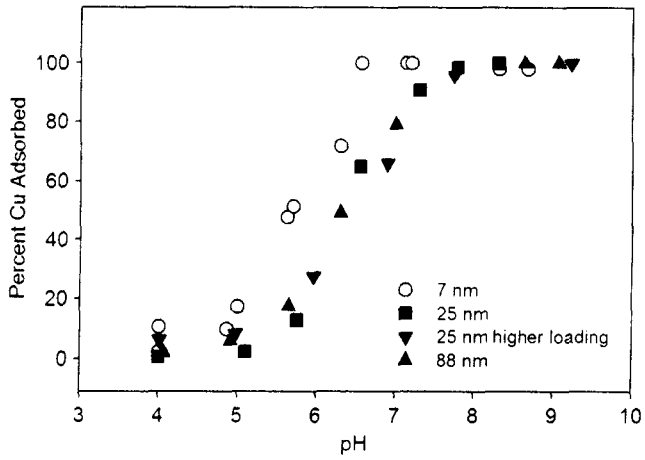

Fig. 3. Batch Cu^{2+} sorption results, normalized for the maximum sorption measured in each experiment.

remaining Fe in solution is extremely small relative to the total amount of sorbed copper (Table EA1). Corrected data are plotted in Fig. 4. Sorption data was corrected for the amount of Fe-bound Cu by converting the mass of Fe (mg/L) into a surface area (m^2/L) using specific surface areas (m^2/g) of each sample. This calculated Fe (hydroxide) surface area was multiplied by the total Cu/total surface area for each experiment (moles/m^2) and a factor accounting for surface—solution distribution at each pH. This factor was calculated using a linear function to describe the sorption edge derived from those samples with Fe below the detection limit (see example for the 7 nm sample as Fig. EA1 in electronic annex EA-1).

Irrespective of the Fe correction, the data clearly indicate a preference in Cu^{2+} binding in the order 7 nm > 25 nm = Fisherbrand (88 nm average diameter). The positions of the edges, as measured at 50% of maximum sorption, shift by approximately 0.6 pH units between experiments with the 7 nm average diameter hematite and all other experiments. The edge positions are qualitatively consistent with other studies of Cu^{2+} sorption on hematite, although the experimental conditions in each design are reflected in the observed edge positions (Christl and Kretzschmar, 1999; Peacock and Sherman, 2004).

Despite tendencies to hydrolyze, dimerize, and form surface precipitates (e.g., Baes and Mesmer, 1986; Palmqvist et al., 1997; Karthikeyan et al., 1999; Strawn et al., 2004), sorption behavior on iron oxides at low to neutral pH, low surface loadings, and low total copper is thought to be adequately described by adsorption alone (Karthikeyan and Elliot, 1999). Adsorption of Cu^{2+} on iron and aluminum oxides occurs instantaneously relative to the timescale of a sorption experiment; however, diffusion along surfaces and into particle aggregates extends the time required to achieve equilibrium (Swallow et al., 1980; Padmanabham, 1983; Grossl et al., 1994; Scheinost et al., 2001; Subramaniam and Yiacoumi, 2001). If diffusion limitation was responsible for causing the differences observed in Cu sorption between the particle sizes, the trend should be opposite—not as much Cu would be sorbed on the smaller particles. Other possible rationalizations such as differences in ionic strength, temperature, surface loading, and total metal added also do not account for the observed trends.

3.3. Zeta potential

Zeta potential results for the hematite samples (0.5 g/L in 0.1 M NaCl) are shown in Fig. 5. The point of zero charge (pzc) is the same within error of the measurements, approximately 8.8. Although there has historically been a very large range in measured values for hematite, for the last 20 years they typically fall in the range of 8.5–9.5, compared with 7.8–7.9 for ferrihydrite (Cornell and Schwertmann, 1996). The 7 nm particles have a higher absolute value of surface potential at any given pH than the 25 nm particles. One possible explanation is the presence of lower-coordinated surface Fe ions. The surface charge of maghemite, the oxidized form of magnetite, is higher

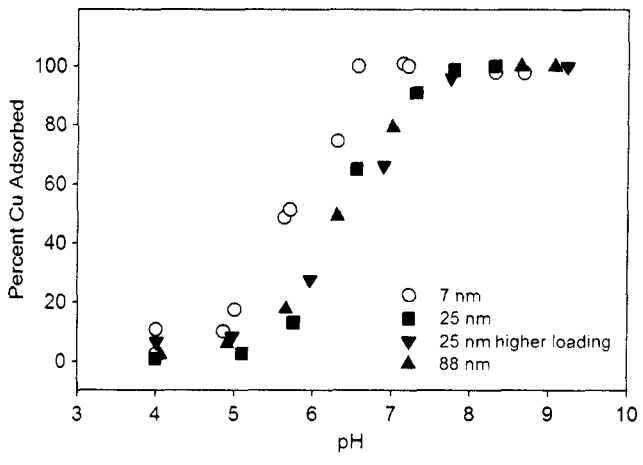

Fig. 4. Normalized batch Cu^{2+} sorption results corrected for iron in analyte solution.

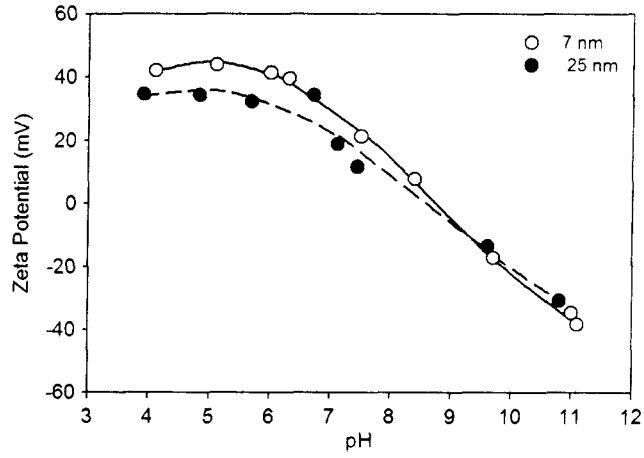

Fig. 5. Zeta potential data for 7 nm and 25 nm hematite.

than that of hematite (Watanabe, 1986). It follows that one possible explanation for the increased surface potential of the 7 nm particles is the presence of undercoordinated iron ions, such as those found in maghemite. The hexagonally close-packed oxygen sublattice of hematite can serve as a template for cubic-close packed magnetite/maghemite domains (Condon, 1998). Multiple surface terminations in domain-like patches have been commonly observed with tunneling microscopy (Wang et al., 1998; Eggleston, 1999; Shaikhutdinov and Weiss, 1999; Eggleston et al., 2003). The pzc of maghemite has been measured to be 6.6 (Garcell et al., 1998) and 6.2 (Jarlbring et al., 2005) due to the higher acidity of certain surface hydroxyl groups relative to those on hematite (Watanabe and Seto, 1993). If maghemite-like domains were present in large amounts on the hematite nanoparticle surfaces, it might be expected that the pzc would shift to a lower value.

The lack of a pzc shift between 7 nm and 25 nm hematites suggests another mechanism may be responsible for differential surface charging. One such hypothesis is that some acute intersections of faces can lead to a higher proton accumulation possibly due to differential solvation near particle edges. Based on molecular modeling of 2–8 nm goethite particles, protons tend to accumulate in these regions. It was suggested that experimentally this effect would be observed as an increase in proton uptake without a large effect on the pzc, which is consistent with the observed zeta potential data (Rustad and Felmy, 2005). Other explanations for the observed zeta potentials include subtle differences in the solution ionic strength or the presence of surface contaminants. Survey scans done with X-ray photoelectron spectroscopy did not reveal the presence of any contaminants other than adventitious carbon.

3.4. Changes in pH-dependent Cu^{2+} binding as a function of size

The pH-dependent adsorption of metal ions on mineral surfaces is controlled by the properties of the ion, the solution, and the surface. The energetics of adsorption can be described as

$$\Delta G^{\circ}_{tot} = \Delta G^{\circ}_{chem} + \Delta G^{\circ}_{coul} \quad (1)$$

in order to separate out the effects of chemical bonding at the surface versus the work done to bring the ion through the potential gradient at the surface (Schindler and Stumm, 1987; Stumm and Morgan, 1996; Sparks, 2003). Observed changes in metal binding as a function of hematite nanoparticle size are likely a result of changes to both components.

The results of the Cu sorption experiments do not support the dominance of electrostatic/coulombic interactions. Although the 7 nm particles have a higher positive surface charge below the pzc, they have a greater affinity for Cu^{2+} ions. However, another consideration is the behavior of water near mineral surfaces. It has been suggested that ion binding on mineral surfaces is related to solvation and hydrolysis (James and Leckie, 1972). When the ion approaches the surface, these terms can be related to dielectric constant of the mineral (Sverjensky and Sal 1996; Sahai and Sverjensky, 1997). Molecular dynam simulations indicate that the dielectric field near the ed of goethite nanoparticles may be heterogeneous, leadi to regions where ions are preferentially solvated (Rust and Felmy, 2005).

The "intrinsic" free energy of adsorption, ΔG°_{chem}, c pends on the distribution of electron density between t metal, surface, and nearby solution. On a heterogeneo surface, sites which are more energetically favorable w have lower ΔG°_{chem}, for example, ΔG°_{chem} (step) $< \Delta G^{\circ}_{che}$ (terrace). In relation to the current study, it is hypothesize that the 7 nm hematite particles have a greater number c surface heterogeneities that are energetically favorable fo Cu^{2+} sorption. The effects of "surface roughness" have of ten been suggested as a reason why electrostatic surfac complexation models are not able to appropriately fit dat (Venema et al., 1998). These surface features likely provid binding environments which stabilize the coordination of Cu^{2+}. The onset of Cu^{2+} sorption at lower pH for 7 nm hematite particles than 25 nm suggests that binding environments which are not present in significant amounts on the larger particles are controlling the sorption behavior onto the 7 nm particles.

3.5. Nature of high-affinity Cu binding sites

Several studies highlight the complex and dynamic nature of hematite surfaces (see Section 1). What is the nature of the binding sites on the 7 nm particles that have higher affinity for Cu^{2+}? Many clues emerge from this work and previous investigations. It is now established that features such as edges, steps and adatoms give rise to most reactivity of surfaces in gas-phase reactions or in vacuum. At these sites, metal ions tend to exist in coordinatively undersaturated environments, where the coordination number of the metal is often lower than in the bulk (Knozinger, 2000). Several studies have documented increases in coordinatively undersaturated metal cations on the surfaces on nanoscale metal oxides, and a general principle seems to be that particles less than 10 nm begin to exhibit significant amounts of coordinatively understaurated surface cations. For example, Zhang et al. (2004) found that single crystal TiO_2 surfaces contained only sixfold coordinated Ti, 6 nm particles had 33% sixfold and 67% fivefold coordinated Ti, and 2 nm particles had 100% fivefold coordinated surface Ti cations. Similar results have been suggested for Fe_2O_3 materials (Chen et al., 2002; Rajh et al., 2002). The ab initio study of Bergermayer et al. (2004) suggests the presence of tetrahedrally coordinated iron atoms at the hematite surface that can be stable under various pO_2 regimes. They relate the prediction of these undercoordinated iron atoms to the STM images of Wang et al. (1998), and assign them a formal oxidation state of +5.

Different principles apply in solution, where oxygen vacancies are filled by reaction with water. However,

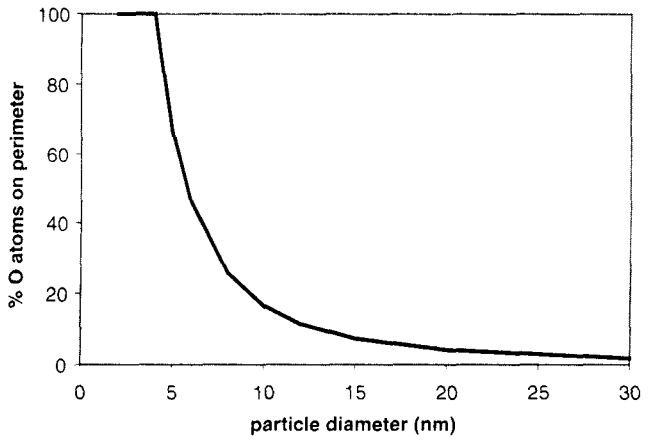

Fig. 6. Percentage of oxygen ions in the crystal calculated to be on the edges, assuming close-packing of 0.13 nm O^{2-} along the extent of the calculated perimeter, as a function of hypothetical hexagonal platelet diameter.

surface ions are still affected by their bonding relationships to the mineral. Sites with crystal chemical variability are still generated near particle edges (Rustad and Felmy, 2005). Assuming that edges can be considered close-packed chains of O^{2-} ions with ionic radius of 0.13 nm, the percentage of edge O^{2-} ions relative to the total number of O^{2-} ions in the crystal is presented in Fig. 6. As the particle diameter becomes smaller than approximately 10 nm (assuming equal width: height ratios to those measured by AFM), edges begin to contribute substantially to the particle surfaces. Considering that the 7 nm average diameter hematite sample used in this study actually contains a large percentage of the size distribution in this range, it is very likely that edge sites with variable Fe—O coordination exist in significantly greater proportion than would on 25 nm or 88 nm hematite particles. It has been previously suggested that Cu^{2+} binding is initiated at step edges on gibbsite (McBride et al., 1984) and at steps and kinks on mica (0001) surfaces (Farquhar et al., 1996).

3.6. Implications for reactivity of metal ions on hematite nanoparticle surfaces

The presence of these sites was hypothesized by Madden and Hochella (2005), who noted that faster oxidation of Mn^{2+} to Mn^{3+} on 7 nm hematite was consistent with the presence of binding environments which stabilize Mn^{3+} (distorted octahedron) relative to Mn^{2+} (perfect octahedron). Changes in metal binding environments clearly have implications for heterogeneous redox reactions, such as Mn^{2+} oxidation. In these cases, adsorption on the mineral surface breaks the metal coordination symmetry, donates electron density, and/or acts as an electron accepting electrode to promote the redox reaction (for example, the reaction between Mn^{2+} and O_2). Using in situ atomic force microscopy, it was observed that on hematite basal planes the MnOOH precipitates that form as a result of heterogeneous Mn^{2+} oxidation in the presence of O_2 always initiated at the base of steps (Junta and Hochella, 1994), and that the most accurate form of a rate law would explicitly include the distribution of topographic features (i.e., binding environments) (Junta-Rosso et al., 1997). Unfortunately, it is not always possible to have direct observations of all the crystal faces involved in a powdered sample, and even more difficult to make these observations on extremely small particles.

Other lines of evidence support the idea that changes in metal coordination have dramatic affects on metal reactivity. Previous studies of the effect of various ligands and aqueous complexes on metal oxidation rates illustrate an equivalent concept (e.g., Wehrli, 1990). For example, there is a direct correlation between the difference in stability constants of ligands for ferric and ferrous iron and the ferric/ferrous redox potential (Table 2). Fig. 7 shows the change in redox potential of iron complexes as a function of the quantity

$$\log K_{eq}\left(\frac{[FeL^{3-n}]}{[Fe^{3+}][L^{n-}]}\right) - \log K_{eq}\left(\frac{[FeL^{2-n}]}{[Fe^{2+}][L^{n-}]}\right). \quad (2)$$

which simply represents the stability of the complex for ferric vs. ferrous iron. Clearly, those complexes which stabilize ferric iron are poor oxidants; they resist the acceptance of an electron. In other words, those ligands

Table 2
Data for Fig. 6 (Stumm and Morgan, 1996; Dhungana and Crumbliss, 2005)

Complexant	log *K*, ferric	log *K*, ferrous	Difference	Eh at pH 7 (V)	Source
Desferrioxamine B	30.6	10.3	20.3	−0.468	a
Exochelin MS	28.86	10.1	18.76	−0.410	a
NTA2			12.7	0.100	b
EDTA	27.7	16.1	11.6	0.120	b
Salicylic acid	17.6	7.4	10.2	0.230	b
CN6	43.6	35.4	8.2	0.430	b
Citric acid	13.5	5.7	7.8	0.600	b

a, Dhungana and Crumbliss (2005); b, Stumm and Morgan (1996).

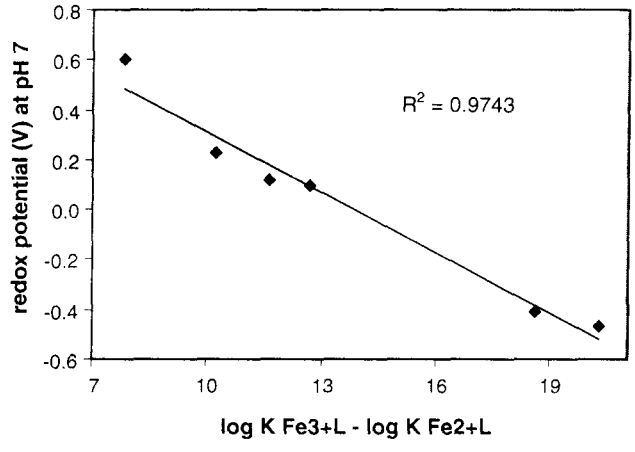

Fig. 7. Relationship between the preference of a ligand for ferric vs. ferrous iron and its redox potential.

encourage the transfer of an electron away from Fe^{2+}. Because the coordination geometry and electronic structure of the iron-ligand complexes to the right of Fig. 7 are more suitable for stabilizing Fe^{3+}, the Fe^{2+}/Fe^{3+} half cell reaction occurs at much lower E_H than with ligands that stabilize Fe^{2+} (left side of Fig. 7).

These relationships between redox potential and coordination environment are directly analogous to the present study. Cu^{2+} ions are most stable in distorted octahedral coordination due to their d-electron configuration, as is also the case for Mn^{3+}. On the other hand, Mn^{2+} is most stable in a symmetric octahedral crystal field. Thus, binding of Mn^{2+} in distorted coordination environments on mineral surfaces stabilizes Mn^{3+} relative to Mn^{2+}, increasing the thermodynamic driving force for the manganese oxidation reaction. Future investigations should explore metal sorption on iron oxide nanoparticles as a function of size using ions without Jahn–Teller distortion such as Co(II) and Ni(II).

4. Summary

The use of Cu^{2+} as a probe metal for hematite nanoparticle surfaces has demonstrated the unique reactivity of nanoscale particles with diameters less than 10 nm. Specifically, the affinity of Cu^{2+} for hematite follows the order 7 nm > 25 nm = 88 nm. In agreement with recent spectroscopic evidence for metal binding on goethite-like nanomaterials (Waychunas et al., 2005), it is suggested that distorted binding environments with reduced symmetry exist in increasing proportion on the surfaces of particles smaller than approximately 10 nm. These sites may be associated with particle edges or other topographic features. Size-dependent changes in the surface structure of nanominerals have implications for the unique reactivity that likely occurs with these materials in the environment, such as interfacial and redox processes.

Acknowledgments

MEEM, Chris Tadanier, Matt Lynch, David Popham, Matt Eick, and Athena Tilley are thanked for helpful discussion or laboratory assistance. The comments of Jim Rustad and three anonymous reviewers significantly improved the manuscript. A.S.M. was supported by the NSF Graduate Research Fellowship program. Funding for this research was from NSF's Nanoscale Science and Engineering (NSE) Program (EAR 01-03053) and the DOE OBES Geosciences Program (DE-FG02-02ER15326).

Associate editor: James R. Rustad

Appendix A. Supplementary data

Supplementary data associated with this article can be found, in the online version, at doi:10.1016/j.gca.2006.06.1366.

References

Alcacio, T.E., Hesterberg, D., Chou, J.W., Martin, J.D., Beauchemin, S., Sayers, D.E., 2001. Molecular scale characteristics of Cu(II) bonding in goethite-humate complexes. *Geochim. Cosmochim. Acta* **65** (9), 1355–1366.

Baes, C.F., Mesmer, R.E., 1986. *Hydrol. Cat.*

Becker, U., Hochella Jr., M.F., Apra, E., 1996. The electronic structure of hematite {001} surfaces: Applications to the interpretation of STM images and heterogeneous surface reactions. *Am. Mineral.* **81** (11–12), 1301–1314.

Becker, U., Rosso, K.M., 2001. Step edges on galena (100): probing the basis for defect driven surface reactivity at the atomic scale. *Am. Mineral.* **86** (7–8), 862–870.

Bergermayer, W., Schweiger, H., Wimmer, E., 2004. Ab initio thermodynamics of oxide surfaces: O_2 on Fe_2O_3(0001). *Phys. Rev. B* **69**, 1–12.

Bigham, J.M., Fitzpatrick, R.W., Schulze, D.G., 2002. Iron Oxides. In: Dixon, J.B., Schulze, D.G. (Eds.), *Soil Mineralogy with Environmental Applications*, vol. 7. Soil Science Society of America.

Borda, M.J., Elsetinow, A.R., Strongin, D.R., Schoonen, M.A., 2003. A mechanism for the production of hydroxyl radical at surface defect sites on pyrite. *Geochim. Cosmochim. Acta* **67** (5), 935–939.

Brown Jr., G.E., Parks, G.A., 2001. Sorption of trace elements on mineral surfaces: modern perspectives from spectroscopic studies, and comments on sorption in the marine environment. *Int. Geol. Rev.* **43**, 963–1073.

Buerge-Weirich, D., Hari, R., Xue, H., Behra, P., Sigg, L., 2002. Adsorption of Cu, Cd, and Ni on goethite in the presence of natural groundwater ligands. *Environ. Sci. Tech.* **36**, 328–336.

Cheah, S.-F., Brown Jr., G.E., Parks, G.A., 2000. XAFS study of Cu model compounds and Cu^{2+} sorption products on amorphous SiO_2, γ-Al_2O_3, and anatase. *Am. Mineral.* **85**, 118–132.

Chen, L.X., Liu, T., Thurnauer, M.C., Csencsits, R., Rajh, T., 2002. Fe_2O_3 nanoparticle structures investigated by X-ray absorption near-edge structure, surface modifications, and model calculations. *J. Phys. Chem. B* **106** (34), 8539–8546.

Chen, L.X., Rajh, T., Wang, Z., Thurnauer, M.C., 1997. XAFS studies of surface structures of TiO_2 nanoparticles and photocatalytic reduction of metal ions. *J. Phys. Chem. B* **101** (50), 10688–10697.

Chiesa, M., Paganini, M.C., Spoto, G., Giamello, E., Di Valentin, C., Del Vitto, A., Pacchioni, G., 2005. Single electron traps at the surface of polycrystalline MgO: assignment of the main trapping sites. *J. Phys. Chem. B.*.

Christl, I., Kretzschmar, R., 1999. Competitive sorption of copper and lead at the oxide–water interface: implications for surface site density. *Geochim. Cosmochim. Acta* **63** (19/20), 2929–2938.

Clementz, D.M., Pinnavia, T.J., Mortland, M.M., 1973. Stereochemistry of hydrated copper(II) ions on the interlamellar surfaces of layer silicates. An electron spin resonance study. *J. Phys. Chem.* **77** (2), 196–200.

Condon, N.G. et al., 1998. Scanning tunnelling microscopy studies of [alpha]-Fe_2O_3. *Surf. Sci.* **397**, 278–287.

Cornell, R.M., Schwertmann, U., 1996. *The Iron Oxides*. VCH.

Criscenti, L.J., Sverjensky, D.A., 1999. The role of electrolyte anions (ClO^{4-}, NO^{3-}, and Cl^{-}) in divalent metal (M^{2+}) adsorption on oxide and hydroxide surfaces in salt solutions. *Am. J. Sci.* **299**, 828–899.

Dhungana, S., Crumbliss, A.L., 2005. Coordination chemistry and redox processes in siderophore-mediated iron transport. *Geomicrobiol. J.* **22**, 87–98.

Eggleston, C.M., 1999. The surface structure of α-Fe_2O_3 (001) by scanning tunneling microscopy: implications for interfacial electron transfer reactions. *Am. Mineral.* **84** (7–8), 1061–1070.

Eggleston, C.M., Stack, A.G., Rosso, K.M., Bice, A.M., 2004. Adatom Fe(III) on the hematite surface: observation of a key reactive surface species. *Geochem. Trans.* **5**, 33.

Eggleston, C.M., Stack, A.G., Rosso, K.M., Higgins, S.R., Bice, A.M., Boese, S.W., Pribyl, R.D., Nichols, J.J., 2003. The structure of

hematite (001) surfaces in aqueous media: scanning tunneling and resonant tunneling calculations of coexisting O and Fe terminations. *Geochim. Cosmochim. Acta* **67** (5), 985–1000.

Elsetinow, A.R., Strongin, D.R., Borda, M.J., Schoonen, M.A., Rosso, K.M., 2003. Characterization of the structure and the surface reactivity of a marcasite thin film. *Geochim. Cosmochim. Acta* **67** (5), 807–812.

Farquhar, M.L., Charnock, J.M., England, E.R., Vaughan, D.J., 1996. Adsorption of Cu(II) on the (0001) plane of mica: a REFLEXAFS and XPS study. *J. Coll. Int. Sci.* **177**, 561–567.

Fernandez-Garcia, M., Martinez-Arias, A., Hanson, J.C., Rodriguez, J.A., 2004. Nanostructured oxides in chemistry: characterization and properties. *Chem. Rev.* **104**, 4063–4104.

Garcell, L., Morales, M.P., Andres-Verges, M., Tartaj, P., Serna, C.J., 1998. Interfacial and rheological characteristics of maghemite aqueous suspensions. *J. Coll. Int. Sci.* **205**, 470–475.

Gilbert, B., Banfield, J.F., 2005. Molecular-scale processes involving nanoparticulate minerals in biogeochemical systems. *Rev. Mineral. Geochem.* **59**, 109–155.

Grossl, P.R., Sparks, D.L., Ainsworth, C.C., 1994. Rapid kinetics of Cu(II) adsorption/desorption on goethite. *Environ. Sci. Tech.* **28**, 1422–1429.

Henderson, M.A., Joyce, S.A., Rustad, J.R., 1998. Interaction of water with the (1 × 1) and (2 × 1) surfaces of hematite (012). *Surf. Sci.* **417**, 66–81.

Henrich, V.E., Cox, P.A., 1996. *The Surface Science of Metal Oxides*. Cambridge University Press.

Hochella Jr., M.F., 1990. Atomic structure, microtopography, composition, and reactivity of mineral surfaces. *Rev. Mineral* **23**, 87–132 (Miner.-Water Interface Geochem.).

Hochella Jr., M.F., 2002. Nanoscience and technology: The next revolution in the Earth sciences. *Earth Planet. Sci. Lett.* **203**, 593–605.

Hochella Jr., M.F., Kasama, T., Putnis, A., Putnis, C.V., Moore, J.N., 2005a. Environmentally important, poorly crystalline Fe/Mn hydrous oxides: ferrihydrite and a possibly new vernadite-like mineral from the Clark Fork River Superfund Complex. *Am. Mineral.* **90**, 718–724.

Hochella Jr., M.F., Moore, J.N., Golla, U., Putnis, A., 1999. A TEM study of samples from acid mine drainage systems: metal–mineral association with implications for transport. *Geochim. Cosmochim. Acta* **63** (19/20), 3395–3406.

Hochella Jr., M.F., Moore, J.N., Putnis, C.V., Putnis, A., Kasama, T., Eberl, D.D., 2005b. Direct observation of heavy metal–mineral association from the Clark Fork River Superfund Complex: implications for metal transport and bioavailability. *Geochim. Cosmochim. Acta* **69** (7), 1651–1663.

James, R.O., Barrow, N.J., 1981. Copper reactions with inorganic components of soils including uptake by oxide and silicate minerals. In: Loneragan, J.F., Robson, A.D., Graham, R.D. (Eds.), *Copper in Soils and Plants*. Academic Press, p. 380.

James, R.O., Leckie, J.O., 1972. Adsorption of hydrolyzable metal ions at the oxide–water interface III. A thermodynamic model of adsorption. *J. Coll. Int. Sci.* **40**, 65–81.

Jarlbring, M., Gunneriusson, L., Hussmann, B., Forsling, W., 2005. Surface complex characteristics of synthetic maghemite and hematite in aqueous suspensions. *J. Coll. Int. Sci.* **285**, 212–217.

Jung, J., Cho, Y.-H., Hahn, P., 1998. Comparitive study of Cu^{2+} adsorption on goethite, hematite, and kaolinite: mechanistic modeling approach. *Bull. Korean Chem. Soc.* **19** (3), 324–327.

Junta, J.L., Hochella Jr., M.F., 1994. Manganese(II) oxidation at mineral surfaces: a microscopic and spectroscopic study. *Geochim. Cosmochim. Acta* **58** (22), 4985–4999.

Junta-Rosso, J.L., Hochella Jr., M.F., 1996. The chemistry of hematite {001} surfaces. *Geochim. Cosmochim. Acta* **60** (2), 305–314.

Junta-Rosso, J.L., Hochella Jr., M.F., Rimstidt, J.D., 1997. Linking microscopic and macroscopic data for heterogeneous reactions illustrated by the oxidation of manganese(II) at mineral surfaces. *Geochim. Cosmochim. Acta* **61** (1), 149–159.

Kabata-Pendias, A., Pendias, H., 1992. *Trace Elements in Soils and Plants*. CRC Press.

Karthikeyan, K.G., Elliot, H.A., 1999. Surface complexation modeling of copper sorption by hydrous oxides of iron and aluminum. *J. Coll. Int. Sci.* **220**, 88–95.

Karthikeyan, K.G., Elliot, H.A., Chorover, J., 1999. Role of surface precipitation in copper sorption by the hydrous oxides of iron and aluminum. *J. Coll. Int. Sci.* **209**, 72–78.

Kim, K.H., Han, H.S., Choi, J.S., 1979. Kintics and mechanisms of the oxidation of carbon monoxide on α-Fe_2O_3. *J. Phys. Chem.* **83** (10), 1286–1289.

Knozinger, H., 2000. Catalysis on oxide surfaces. *Science* **287**, 1407–1409.

Liu, P., Kendelewicz, T., Brown Jr., G.E., 1998a. Reaction of water with MgO(100) surfaces. Part II: synchrotron photoemission studies of defective surfaces. *Surf. Sci.* **412–413**, 315–332.

Liu, P., Kendelewicz, T., Brown, G.E., Nelson, E.J., Chambers, S.A., 1998b. Reaction of water vapor with α-Al_2O_3(0001) and α-Fe_2O_3(0001) surfaces: synchrotron X-ray photoemission studies and thermodynamic calculations. *Surf. Sci.* **417** (1), 53–65.

Madden, A.S., Hochella Jr., M.F., 2005. A test of geochemical reactivity as a function of mineral size: manganese oxidation promoted by hematite nanoparticles. *Geochim. Cosmochim. Acta* **69** (2), 389–398.

McBride, M.B., 1981. Forms and distribution of copper in solid and solution phases of soil. In: Loneragan, J.F., Robson, A.D., Graham, R.D. (Eds.), *Copper in Soils and Plants*. Academic Press, p. 380.

McBride, M.B., 1989. Reactions controlling heavy metal solubility in soils. *Adv. Soil Sci.* **10**, 1–47.

McBride, M.B., Fraser, A.R., McHardy, W.J., 1984. Cu^{2+} interaction with microcrystalline gibbsite. Evidence for oriented chemisorbed copper ions. *Clays Clay Min.* **32** (1), 12–18.

Padmanabham, M., 1983. Adsorption-desorption behavior of copper(II) at the goethite-solution interface. *Australian J. Soil Res.* **21**, 309–320.

Palmqvist, U., Ahlberg, E., Lovgren, L., Sjoberg, S., 1997. *In situ* voltammetric determinations of metal ions in goethite suspensions: single metal ion systems. *J. Coll. Int. Sci.* **196**, 254–266.

Parkman, R.J., Charnock, J.M., Bryan, N.D., Livens, F.R., Vaughan, D.J., 1999. Reactions of copper and cadmium ions in aqueous solution with goehite, lepidocrocite, mackinawite, and pyrite. *Am. Mineral.* **84**, 407–419.

Peacock, C.L., Sherman, D.M., 2004. Copper(II) sorption onto goethite, hematite and lepidocrocite: a surface complexation model based on ab initio molecular geometries and EXAFS spectroscopy. *Geochim. Cosmochim. Acta* **68** (12), 2623–2637.

Pecharroman, C., Gonzalez-Carreno, T., Iglesias, J.E., 1995. The infrared dielectric properties of maghemite, gamma-Fe_2O_3, from reflectance measurement on pressed powders. *Phys. Chem. Min.* **22**, 21–29.

Rajh, T., Chen, L.X., Lukas, K., Liu, T., Thurnauer, M.C., Tiede, D.M., 2002. Surface restructuring of nanoparticles: an efficient route for ligand–metal oxide crosstalk. *J. Phys. Chem. B* **106** (41), 10543–10552.

Rose, A.W., Bianchi-Mosquera, G.C., 1993. Adsorption of Cu, Pb, Zn, Co, Ni, and Ag on goethite and hematite: A control on metal mobilization from red beds into stratiform copper deposits. *Econ. Geol.* **88**, 1226–1236.

Rosso, K.M., 2001. Structure and reactivity of semiconducting mineral surfaces: convergence of molecular modeling and experiment. *Rev. Mineral. Geochem.* **42**, 199–271 (Molecular Modeling Theory).

Rosso, K.M., Becker, U., Hochella Jr., M.F., 2000. Surface defects and self-diffusion on pyrite {100}: an ultra-high vacuum scanning tunneling microscopy and theoretical modeling study. *Am. Mineral.* **85** (10), 1428–1436.

Rustad, J.R., Felmy, A.R., 2005. The influence of edge sites on the development of surface charge on goethite nanoparticles: a molecular dynamics investigation. *Geochim. Cosmochim. Acta* **69** (6), 1405–1412.

Sadykov, V.A., Tikhov, S.F., Tsybulya, S.V., Kryukova, G.N., Veniaminov, S.A., Kolomiichuk, V.N., Bulgakov, N.N., Paukshtis, E.A., Ivanov, V.P., Koshcheev, S.V., Zaikovskii, V.I., Isupova, L.A., Burgina, L.B., 2000. Role of defect structure in structural sensitivity of the oxidation reactions catalyzed by dispersed transition metal oxides. *J. Mol. Catal. A* **158**, 361–365.

Sahai, N., Sverjensky, D.A., 1997. Solvation and electrostatic model for specific electrolyte adsorption. *Geochim. Cosmochim. Acta* **61** (14), 2827–2848.

Samson, S.D., Eggleston, C.M., 1998. Active sites and the non-steady-state dissolution of hematite. *Environ. Sci. Tech.* **32**, 2871–2875.

Samson, S.D., Eggleston, C.M., 2000. The depletion and regeneration of dissolution-active sites at the mineral–water interface: II. Regeneration of active sites on α-Fe_2O_3 at pH 3 and pH 6. *Geochim. Cosmochim. Acta* **64** (21), 3675–3683.

Scheinost, A.C., Abend, S., Pandya, K.I., Sparks, D.L., 2001. Kinetic controls on Cu and Pb sorption by ferrihydrite. *Environ. Sci. Tech.* **35**, 1090–1096.

Schindler, P.W., Stumm, W., 1987. The surface chemistry of oxides, hydroxides, and oxide minerals. In: Stumm, W. (Ed.), *Aquatic Surface Chemistry: Chemical Processes at the Particle–Water Interface*. Wiley, pp. 83–110.

Schwertmann, U., Cornell, R.M., 2000. *Iron Oxides in the Laboratory*. Wiley-VCH.

Shaikhutdinov, S.K., Weiss, W., 1999. Oxygen pressure dependence of the α-Fe_2O_3(0001) surface structure. *Surf. Sci.* **432**, L627–L634.

Sparks, D.L., 2003. *Environmental Soil Chemistry*. Academic Press.

Sposito, G., 1989. *The Chemistry of Soils*. Oxford University Press.

Stirnman, M.J., Huang, C., Smith, R.S., Joyce, S.A., Kay, B.D., 1996. The adsorption and desorption of water on single crystal Mg(100): the role of surface defects. *J. Chem. Phys.* **105** (3), 1295–1298.

Strawn, D.G., Palmer, N.E., Funare, L.J., Goodell, C., Amonette, J.E., Kukkadapu, R.K., 2004. Copper sorption mechanisms on smectites. *Clays Clay Min.* **52** (3), 321–333.

Stumm, W., Morgan, J., 1996. *Aquatic Chemistry*. John Wiley & Sons.

Subramaniam, K., Yiacoumi, S., 2001. Modeling kinetics of copper uptake by inorganic colloids under high surface coverage conditions. *Coll. Surf. A* **191**, 145–159.

Sverjensky, D.A., Sahai, N., 1996. Theoretical prediction of single-site surface-protonation equilibrium constants for oxides and silicates in water. *Geochim. Cosmochim. Acta* **60**, 3773–3797.

Swallow, K.C., Hume, D.N., Morel, F.M.M., 1980. Sorption of copper and lead by hydrous ferric oxide. *Environ. Sci. Tech.* **14** (11), 1326–1331.

Trainor, T.P., Chaka, A.M., Eng, P.J., Newville, M., Waychunas, G.A., Catalano, J.G., Brown, G.E., 2004. Structure and reactivity of the hydrated hematite (0001) surface. *Surf. Sci.* **573** (2), 204–224.

Venema, P., Hiemstra, T., Weidler, P.G., van Riemsdijk, W.H., 1998. Instrinsic proton affinity of reactive surface groups of metal (hydr)oxides: application to iron (hydr)oxdies. *J. Coll. Int. Sci.* **198**, 282–295.

Wang, X.G., Weiss, W., Shaikhutdinov, Sh.K., Ritter, M., Petersen, M., Wagner, F., Schlögl, R., Scheffler, M., 1998. The hematite (0001) surface: evidence for domains of distinct chemistry. *Phys. Rev. Lett.* **81** (5), 1038–1041.

Watanabe, H., 1986. The point of zero charge and the isoelectric point of γ-Fe_2O_3 and α-Fe_2O_3. *Bull. Chem. Soc. Japan* **59**, 2683–2687.

Watanabe, H., Seto, J., 1993. Specific acidities of the surface hydroxyl groups on maghemite. *Bull. Chem. Soc. Japan* **66**, 395–399.

Waychunas, G.A., 2001. Structure, aggregation, and characterization of nanomaterials. *Rev. Mineral. Geochem.* **44**, 105–166.

Waychunas, G.A., Kim, C.S., Banfield, J.F., 2005. Nanoparticulate iron oxide minerals in soils and sediments: unique properties and contaminant scavenging mechanisms. *J. Nanoparticle Res.* **7**, 409–433.

Wehrli, B., 1990. Redox reactions of metal ions at mineral surfaces. In: Stumm, W. (Ed.), *Aquatic Chemical Kinetics*. pp. 311–336.

Xia, K., Bleam, W., Helmke, P.A., 1997. Studies of the nature of Cu^{2+} and Pb^{2+} binding sites in soil humic substances using X-ray absorption spectroscopy. *Geochim. Cosmochim. Acta* **61** (11), 2211–2221.

Zhang, J., Wu, Z.Y., Ibrahim, W., Abbas, M.I., Ju, X., 2003. Surface structure of α-Fe_2O_3 nanocrystal observed by O K-edge X-ray absorption spectroscopy. *Nucl. Inst. Meth. Phys. Res. B* **199**, 291–294.

Zhang, Q., Du, L., Weng, Y., Wang, L., Chen, H., Li, J., 2004. Particle-size dependent distribution of carboxylate adsorption sites on TiO_2 nanoparticle surfaces: insights into the surface modification of nanostructured TiO_2 electrodes. *J. Phys. Chem. B* **108**, 15077–15083.